Instability of a thin film flowing on a rotating horizontal or inclined plane

L. A. Dávalos-Orozco
Instituto de Investigaciones en Materiales, Universidad Nacional Autónoma de México, Ciudad Universitaria, Apartado Postal 70-360, Delegación Coyocán, 04510 México Distrito Federal, Mexico

F. H. Busse
Physikalisches Institut, Universität Bayreuth, D-95440 Bayreuth, Germany
(Received 20 August 2001; published 25 January 2002)

In this paper the instability of a thin fluid film flowing under the effects of gravity, Coriolis, and centrifugal forces is investigated. It is supposed that the film flows far from the axis of rotation on a plane which may be horizontal or inclined with respect to the horizontal. In the former case, the flow is only driven by the centrifugal force while in the latter case, the flow is driven by the components of centrifugal force and gravity along the plane. This case may also be considered as the flow down a rotating cone but far from the apex. The stabilizing influence of rotation on the film flow increases with the rotation rate. Up to a certain critical rate of rotation, the film flowing down the rotating inclined plane (or cone) is more stable than the flow on the horizontal rotating plane while above this rate of rotation the situation is reversed. The instability above the critical rate is associated with a finite wave number in contrast to the vanishing wave number of the instability below the critical rate. The possibility of Ekman layer instabilities is also investigated. An equation describing the nonlinear evolution of surface waves is also obtained. Moreover, this equation is simplified for the case in which the amplitudes are very small. An equation including dissipation as well as dispersion is derived whose solutions may possess solitary waves, as in the case of similar equations considered in the literature. These solutions are likely to correspond to the solitary spiral waves observed in experiments.

DOI: 10.1103/PhysRevE.65.026312 PACS number(s): 47.15.Fe, 47.20.−k, 47.32.−y, 47.35.+i

I. INTRODUCTION

The instability of fluid layers coating a surface is a problem of concern in many industrial applications where the finishing should be smooth. Therefore, this problem has been investigated for many years in order to understand the behavior of thin liquid films in motion. Benjamin [1] investigated theoretically the linear instability of a thin film flowing down an incline. The presentation of his results was simplified by Yih [2], who also considered separately the limit of small wave numbers and small Reynolds numbers. An equation for waves of finite amplitude with the small wave number approximation was derived by Benney [3]. This equation is highly nonlinear and has been reduced, by means of the small amplitude approximation, to the Kuramoto-Sivashinsky equation [4,5].

The possibility of propagation of solitary waves on thin films down an inclined plane was first confirmed theoretically by Pumir *et al.* [6] by means of the Benney equation. Later, using the reference frame moving with the solitary wave, Nakaya [7] solved the stationary Benney equation as a boundary value problem. He proposed a selection rule to determine which kind of solitary wave really appears.

Numerical analysis of the Benney equation by means of Fourier spectral methods has been done in two dimensions by Joo *et al.* [8] and in three dimensions by Joo and Davis [9]. Finite differences were used by Dávalos-Orozco *et al.* [10] to obtain a solution of the Benney equation which includes an extra term of an external perturbation equivalent to a local sinusoidal pressure fluctuation.

Numerous experiments on films flowing down inclined planes have been performed in recent years. Liu and Gollub [11] investigated the transition to turbulence and later (Liu and Gollub [12]) studied the appearance and interaction of solitary waves. Three-dimensional waves and their evolution towards solitary waves were investigated by Liu *et al.* [13].

The flow on a rotating horizontal disk has been investigated by several authors. Depending on whether the fluid is injected from above or below the rotating disk, different theoretical and experimental results have been obtained. Charwat *et al.* [14] have measured the thickness and stability of the thin film on a horizontal disk rotating about its vertical axis and compared their results with an asymptotic solution. Their experiments showed circular and spiral waves besides irregular waves. From their linear analysis they obtained the result that disturbances propagating at an angle with respect to the radial direction are most unstable. They found agreement with the measured angle of the spiral waves in their experiment. Rauscher *et al.* [15] presented asymptotic solutions for the thin film including various effects like surface curvature and surface tension. Needham and Merkin [16] developed a theory for the nonlinear description of localized disturbances on a steady film. They were interested in entrance effects and they used matched asymptotic expansions. They also discussed the conditions for the instability of the film. Experiments have also been done by Azuma and Nunobe [17] who were concerned with the dependence of the stability on the input flow rate and on the height above the rotating disk of the discharging circular tube. They observed persistent perturbations presumably generated by the tube. Similar experiments have been done more recently by Leneweit *et al.* [18]. Supposing that the entrance acts as a periodic wave generator they present, systematically for various flow rates, results obtained through varying the height of the tube nozzle above the disk.

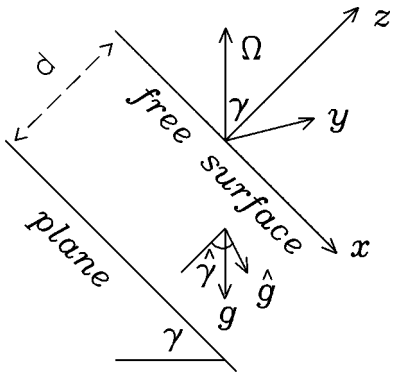

FIG. 1. Sketch of the geometrical configuration for the fluid film down a rotating inclined rigid plane or cone. The rotating horizontal disk is obtained when $\gamma=0°$.

The instability of a thin film resulting from a combination of inclination and rotation was first investigated by Dávalos-Orozco and Ruiz-Chavarría [19]. They assumed a fluid flowing down a rotating inclined plane close to the axis of rotation, in order to neglect centrifugal effects. The linear instability of the film was described in the limit of small wave numbers and small Reynolds numbers. A stabilizing effect of the Coriolis force was found.

In the case of a rotating inclined plane, the centrifugal force can be introduced in the same way as done by Hoffmann and Busse [20] for the problem of flow inside two parallel coaxial rotating cones. It is supposed that the flow is investigated in a region very far from the apices and that the cones can be approximated as plane and parallel plates. The rotation vector thus makes an angle γ with respect to the normal of the plates. This procedure is applied in the present paper. The mathematical formulation of the problem and the basic flow are presented in Sec. II. After the linear instability is discussed in Sec. III, the Ekman layer instability is investigated in Sec. IV. The nonlinear problem is studied in Sec. V and a nonlinear evolution equation of the Benney type is derived to describe the thin film surface deformation for small rotation parameter. The paper ends with the conclusions in Sec. VI.

II. DESCRIPTION OF THE SYSTEM AND EQUATIONS OF MOTION

The system under investigation is a thin film flowing down a plane which is inclined with an angle γ with respect to the horizontal and rotating about a vertical axis as shown in Fig. 1. The origin of the coordinate system is fixed at the unperturbed free surface of the film with the x and y axes parallel to the surface and the z axis perpendicular to it. In the absence of rotation the basic flow is parallel to the x axis. The angular velocity vector $\vec{\Omega}$ has the components $\Omega_x=-|\vec{\Omega}|\sin\gamma$ and $\Omega_z=|\vec{\Omega}|\cos\gamma$. The acceleration of gravity has the x and z components $g\sin\gamma$ and $g\cos\gamma$. In this sense, the problem can be regarded as an approximation for a thin film flowing down a rotating cone at a position sufficiently far from the apex. For a vanishing angle of inclination γ the limit of a rotating horizontal plane is obtained.

The motion is described by the Navier-Stokes and continuity equations for an incompressible fluid in a system of coordinates fixed to the rotating plane. They are

$$\rho\left[\frac{\partial\vec{u}}{\partial t}+\vec{u}\cdot\vec{\nabla}\vec{u}+2\vec{\Omega}\times\vec{u}+\vec{\Omega}\times(\vec{\Omega}\times\vec{r})\right]$$
$$=-\vec{\nabla}p+\rho\vec{g}+\rho\nu\nabla^2\vec{u}, \tag{1}$$

$$\vec{\nabla}\cdot\vec{u}=0, \tag{2}$$

where ρ is the density, $\vec{u}=(u,v,w)$ is the velocity vector, p is the pressure, and ν is the kinematic viscosity. The Coriolis acceleration has three components,

$$2\vec{\Omega}\times\vec{u}=2|\vec{\Omega}|(-v\cos\gamma,u\cos\gamma,-v\sin\gamma), \tag{3}$$

while the centrifugal force is given by

$$\vec{\Omega}\times\vec{\Omega}\times\vec{r}_0=-r_0|\vec{\Omega}|^2(\cos\gamma,0,\sin\gamma), \tag{4}$$

where $\overline{r_0}=x_0\cos\gamma+z_0\sin\gamma$. For simplicity we restrict the attention to angles γ in the interval $0\leqslant\gamma\leqslant90°$ corresponding to a positive sense of rotation.

Centrifugal force and gravity can be combined into an effective gravity vector

$$\vec{g}_e=\sqrt{g^2+\overline{r_0}^2|\vec{\Omega}|^4}\,(\sin\hat{\gamma},0,\cos\hat{\gamma}) \tag{5}$$

with

$$\sin\hat{\gamma}=\frac{g\sin\gamma+\overline{r_0}|\vec{\Omega}|^2\cos\gamma}{\sqrt{g^2+\overline{r_0}^2|\vec{\Omega}|^4}},$$

$$\cos\hat{\gamma}=\frac{g\cos\gamma-\overline{r_0}|\vec{\Omega}|^2\sin\gamma}{\sqrt{g^2+\overline{r_0}^2|\vec{\Omega}|^4}}. \tag{6}$$

The thus defined angle $\hat{\gamma}$ describes the direction of $\vec{g}_e$ in the x,z plane. In order to avoid separation of the film from the plane $\hat{\gamma}<90°$, i.e., $\tan\gamma<g/\overline{r_0}|\vec{\Omega}|^2$ must be required.

Assuming d, d^2/ν, ν/d, and $\rho(\nu/d)^2$, as scales for length, time, velocity, and pressure, respectively, we write the equations of motion in dimensionless form,

$$\frac{\partial u}{\partial t}+\vec{u}\cdot\vec{\nabla}u-2\chi^2v=-\frac{\partial p}{\partial x}+\nabla^2u+\mathrm{Re}, \tag{7}$$

$$\frac{\partial v}{\partial t}+\vec{u}\cdot\vec{\nabla}v+2\chi^2(w\tan\gamma+u)=-\frac{\partial p}{\partial y}+\nabla^2v, \tag{8}$$

$$\frac{\partial w}{\partial t}+\vec{u}\cdot\vec{\nabla}w-2\chi^2v\tan\gamma=-\frac{\partial p}{\partial z}+\nabla^2w-\mathrm{Re}\cot\hat{\gamma}, \tag{9}$$

$$\vec{\nabla}\cdot\vec{u}=0, \tag{10}$$

where Re and χ^2 are defined by $\mathrm{Re}=\sqrt{g^2+\vec{r}_0^{\,2}|\vec{\Omega}|^4}\sin\hat{\gamma}d^3/\nu^2$ and $\chi^2=\Omega\cos\gamma$ with the rotation parameter given by $\Omega=|\vec{\Omega}|d^2/\nu$. The boundary condition at the rigid lower plane is given by

$$\vec{u}=0 \quad \text{at } z=-1. \tag{11}$$

At $z=H$, where H is the deviation from $z=0$ of the free surface, the normal and the tangential stresses are

$$\begin{aligned}-p+&\left[\frac{\partial u}{\partial x}H_x^2+\frac{\partial v}{\partial y}H_y^2+\left(\frac{\partial u}{\partial y}+\frac{\partial v}{\partial x}\right)H_xH_y-\left(\frac{\partial v}{\partial z}+\frac{\partial w}{\partial y}\right)H_y\right.\\&\left.-\left(\frac{\partial u}{\partial z}+\frac{\partial w}{\partial x}\right)H_x+\frac{\partial w}{\partial z}\right](1+H_x^2+H_y^2)^{-1}\\&=\Sigma[(1+H_y^2)H_{xx}+(1+H_x^2)H_{yy}\\&\quad-2H_xH_yH_{xy}](1+H_x^2+H_y^2)^{-3/2},\end{aligned} \tag{12}$$

$$\begin{aligned}&\left(\frac{\partial w}{\partial z}-\frac{\partial u}{\partial x}\right)H_x-\frac{1}{2}\left(\frac{\partial u}{\partial y}+\frac{\partial v}{\partial x}\right)H_y+\frac{1}{2}\left(\frac{\partial u}{\partial z}+\frac{\partial w}{\partial x}\right)(1-H_x^2)\\&\quad-\frac{1}{2}\left(\frac{\partial w}{\partial y}+\frac{\partial v}{\partial z}\right)H_xH_y=0,\end{aligned} \tag{13}$$

$$\begin{aligned}&\left(\frac{\partial w}{\partial z}-\frac{\partial v}{\partial y}\right)H_y-\frac{1}{2}\left(\frac{\partial u}{\partial y}+\frac{\partial v}{\partial x}\right)H_x-\frac{1}{2}\left(\frac{\partial u}{\partial z}+\frac{\partial w}{\partial x}\right)H_xH_y\\&\quad+\frac{1}{2}\left(\frac{\partial v}{\partial z}+\frac{\partial w}{\partial y}\right)(1-H_y^2)=0,\end{aligned} \tag{14}$$

where Σ is the capillary number, $\Sigma=\sigma d/\rho\nu^2$, with the surface tension σ. The distortion H must satisfy the kinematic boundary condition

$$w=\frac{\partial H}{\partial t}+uH_x+vH_y. \tag{15}$$

where H_x and H_y indicate partial derivative of H with respect to x and y.

The solutions for the basic flow are given by the x,y, and t independent solutions $u=U$, $v=V$ of Eqs. (7)–(10) which can be written in the complex form $F=U+iV$,

$$F=U+iV=iG\left(\frac{\cosh(1+i)\chi z}{\cosh(1+i)\chi}-1\right), \tag{16}$$

where $G=\mathrm{Re}/2\chi^2$. The nondimensional flow rate $Q=\int_{-1}^{0}U\,dz$ is

$$Q=\frac{G}{2\chi}\,\frac{\sinh\chi\cosh\chi-\sin\chi\cos\chi}{\cosh^2\chi-\sin^2\chi}. \tag{17}$$

Note that it is proportional to the Reynolds number, but depends in a complex way on rotation. In fact, in the limit of $\chi\to0$, $Q\to\mathrm{Re}(1/3-68\chi^4/315)$. The pressure P is obtained through integration of Eq. (9). Some graphs of U and V for different values of χ can be found in the paper by Dávalos-Orozco and Ruiz-Chavarría [19].

III. LINEAR STABILITY ANALYSIS

In this section the stability of the basic flow Eq. (16) is investigated with respect to infinitesimal perturbations. For this purpose, the linearized versions of Eqs. (7) to (15) are solved with a shooting method [21]. The perturbation of the velocity vector is introduced through the general representation for a solenoidal field $\vec{u}=\vec{\nabla}\times\vec{\nabla}(\hat{k}\phi)+\vec{\nabla}\times(\hat{k}\psi)$ where $\hat{k}$ is the unit vector in the z direction. The potentials ϕ and ψ have a representation in normal modes of the form $f(z)\exp[ia(x\cos\varepsilon-y\sin\varepsilon-ct)]$ where ε is the angle of propagation of the perturbation with respect to the x direction. Since we use a right-handed coordinate system with the x coordinate in the radial direction the fluid film has a negative component of velocity V in the y direction and a positive angle ε must be expected in general.

Critical Reynolds numbers for instability as a function of the rotation parameter have been computed for selected values of $\hat{\gamma}$, γ, and Σ. The corresponding critical values of the wave number, the phase velocity, and the angle ε can be used to infer some typical properties of the instabilities.

As is evident from the variation of Re with Ω in Figs. 2(a), 3(a), and 4(a), rotation strongly inhibits the onset of instability. For low values of Ω the instability occurs in the form of long wavelength waves in the same way as in the nonrotating inclined layer where the critical wave number also vanishes. The angle ε increases from zero with Ω as shown in Figs. 2(b), 3(b), and 4(b). The long-wave instability is replaced by an instability with finite values of the wave number a when Ω exceeds a certain critical value which increases with the parameter $\hat{\gamma}$. This change in the character of the instability is also reflected in Re, ε, and c, as shown in the figures. It is of interest to see that the flow down a rotating inclined plane is slightly more stable than that on a horizontal plane in the case of the long wavelength instability. The reverse is found for the finite wave number instability.

Typical results for the functions ϕ and ψ are shown in Fig. 5. The form of the function does not change much with γ and only representative examples have been plotted to exhibit the dependence on Ω. In the small wave number limit the amplitudes of ϕ and ψ can be chosen such that the imaginary parts vanish. In the small wave number approximation the amplitude of ψ increases with Ω relative to the amplitude of ϕ. As the mode with a finite critical wave number becomes preferred the form of the functions ϕ and ψ changes and the u_y component of the disturbance velocity shifts in phase by nearly 90° relative to the u_x component owing to the high value of the frequency of oscillation. The typical form of the functions ϕ and ψ at a high value of Ω is shown in the third plot of the figure. The fourth plot shows the dependence on z of ϕ and ψ in the case of the Ekman layer instability.

For small wave numbers a and χ the results agree with the analytical expressions obtained by Charwat *et al.* [14] for a rotating horizontal plane. Using the linearized version of the nonlinear equation derived in Sec. V we present here analytical stability results for arbitrary γ assuming a surface deformation of the form $H=H_0\exp[ia(x\cos\varepsilon-y\sin\varepsilon-ct)+\Gamma t]$. In this way we obtain from the nonlinear Eq. (31) in the small wave number and small χ approximation the following

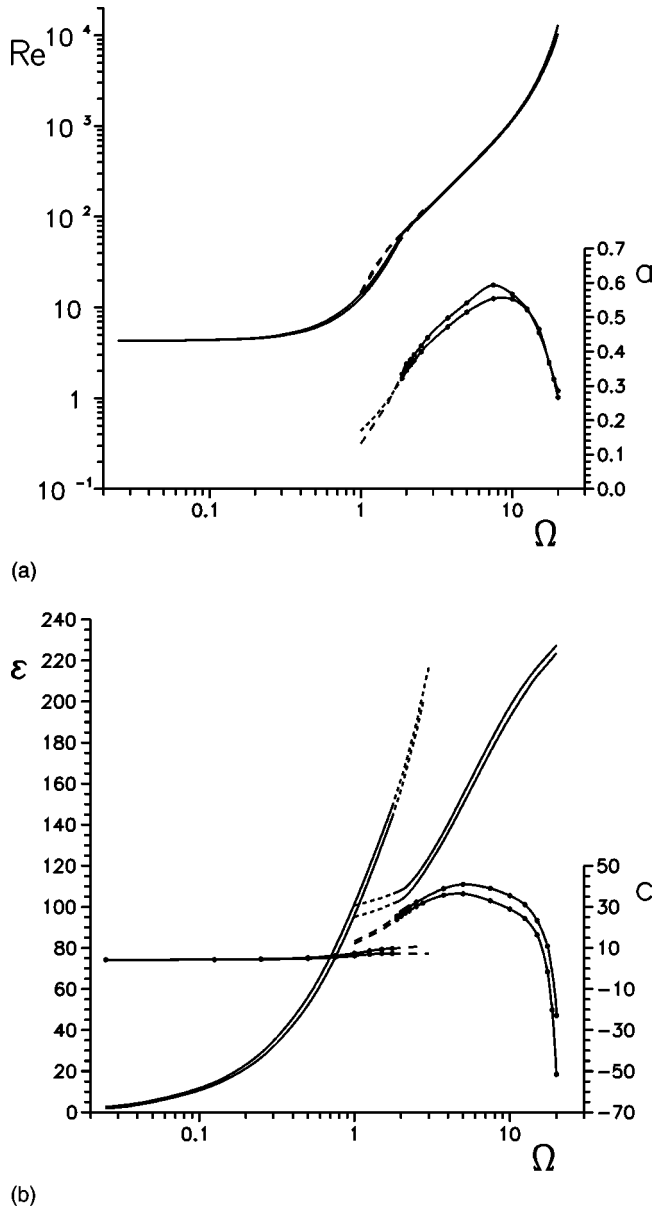

FIG. 2. (a) The critical Reynolds number Re (solid curves, left ordinate) and the critical wave number a (starred curve, right ordinate) as a function of the rotation parameter Ω in the case of $\hat{\gamma}=30°$, $\Sigma=500$. The critical wave number a vanishes for $\Omega \lesssim 1.75$ where the mode of instability changes. In order to indicate the crossing more clearly the Reynolds number and other properties have been extended by dashed lines here and in the following figures into the region where the mode is no longer critical. The upper (lower) curve of Re corresponds to $\gamma=20°$ (0°) for $\Omega \lesssim 1.75$. For $\Omega \gtrsim 1.75$ the upper (lower) curve of Re as well as of a corresponds to $\gamma=0°$ (20°). (b) The angle ε (solid curves) and the plane velocity c (starred curve) for the same cases as in (a). The upper (lower) curves correspond to $\gamma=0°$ (20°) in the case of ε and to $\gamma=20°$ (0°) in the case of c.

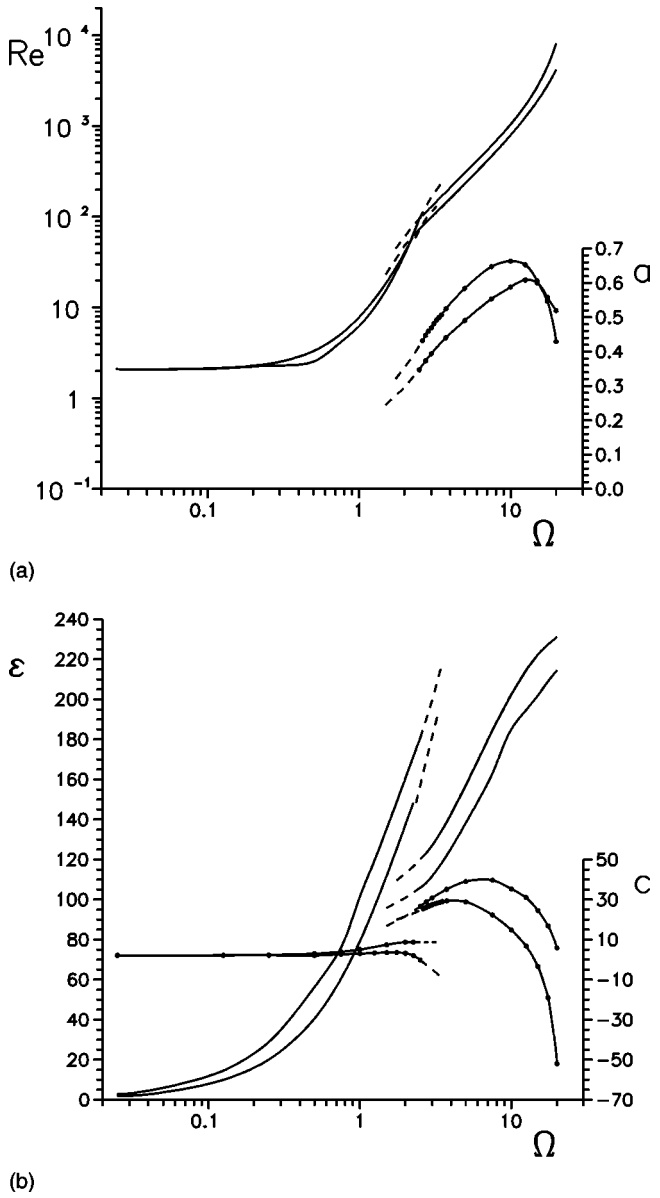

FIG. 3. (a) Same as Fig. 2(a) except that $\hat{\gamma}=50°$ has been used. The upper and lower curves of Re correspond to $\gamma=40°$ for $\Omega \lesssim 2.25$ and to $\gamma=0°$ for $\Omega \lesssim 2.5$, respectively. For $\Omega \gtrsim 2.5$ the upper curve of Re as well as of a corresponds to $\gamma=0°$ and for $\Omega \gtrsim 2.25$ the lower curve of Re as well as of a corresponds to $\gamma=40°$. (b) Same as Fig. 2(b) except that $\hat{\gamma}=50°$ has been used. The upper (lower) curves correspond to $\gamma=0°$ (40°) in the case of ε and to $\gamma=40°$ (0°) in the case of c.

nondimensional phase velocity c and growth rate Γ:

$$c=\mathrm{Re}(\cos\varepsilon+\tfrac{4}{3}\chi^2\sin\varepsilon)+\tfrac{8}{45}\chi^2 a^2\mathrm{Re}\sin\varepsilon, \qquad (18)$$

$$\Gamma=a^2[\tfrac{2}{15}\mathrm{Re}^2\cos^2\varepsilon-\tfrac{1}{3}\mathrm{Re}\cot\hat{\gamma}-\tfrac{1}{3}\Sigma a^2 + \chi^2\sin\varepsilon\cos\varepsilon(\tfrac{4}{7}\mathrm{Re}^2-\tfrac{3}{20}\mathrm{Re}\tan\gamma)]. \qquad (19)$$

The last term of Eq. (18) arises from the first order in the expansion and is a dispersion contribution to the phase velocity due to the presence of rotation.

The angle ε of maximum growth is given by

$$\tan 2\varepsilon=\chi^2\left(\frac{30}{7}-\frac{9}{8}\frac{\tan\gamma}{\mathrm{Re}}\right) \qquad (20)$$

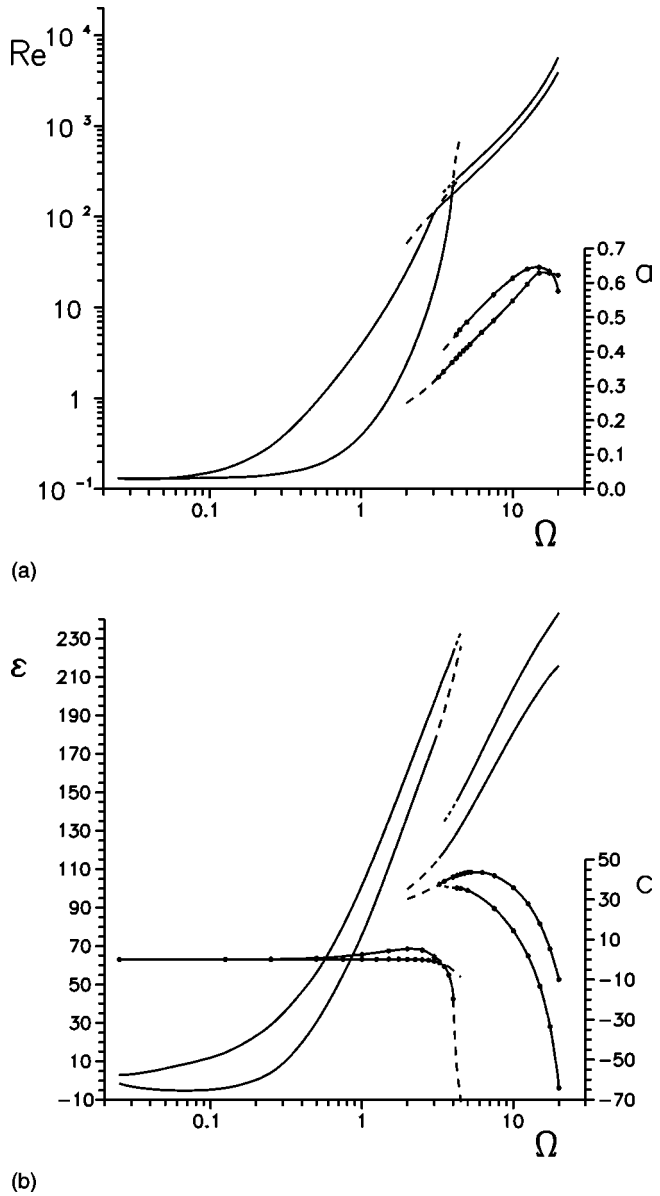

FIG. 4. (a) Same as Fig. 2(a) except that $\hat{\gamma}=87°$ and $\Sigma=2500$ has been used. The upper and lower curves of Re correspond to $\gamma=40°$ for $\Omega\lesssim 3$ and to $\gamma=0°$ for $\Omega\lesssim 4$, respectively. For $\Omega\gtrsim 4$ the upper curve of Re as well as of a corresponds to $\gamma=0°$ and for $\Omega\gtrsim 3$ the lower curve of Re as well as of a corresponds to $\gamma=40°$. (b) Same as Fig. 2(b) except that $\hat{\gamma}=87°$ and $\Sigma=2500$ has been used. The upper (lower) curves correspond to $\gamma=0°$ (40°) in the case of ε and to $\gamma=40°$ (0°) in the case of c. Note that ε for $\gamma=40$ remains negative up to $\Omega\lesssim 0.12$.

which depends on Re and γ.

The general expression for the critical Reynolds number at which Γ vanishes is rather complex and will not be given here [see Eq. (37)]. Instead we shall discuss particular cases.

For $\Sigma=0$ or for a very small, the critical Reynolds number is

$$\mathrm{Re}_c=\frac{\frac{1}{3}\cot\hat{\gamma}+\frac{3}{20}\chi^2\tan\gamma\sin\varepsilon\cos\varepsilon}{\frac{2}{15}\cos^2\varepsilon+\frac{4}{7}\chi^2\sin\varepsilon\cos\varepsilon}. \tag{21}$$

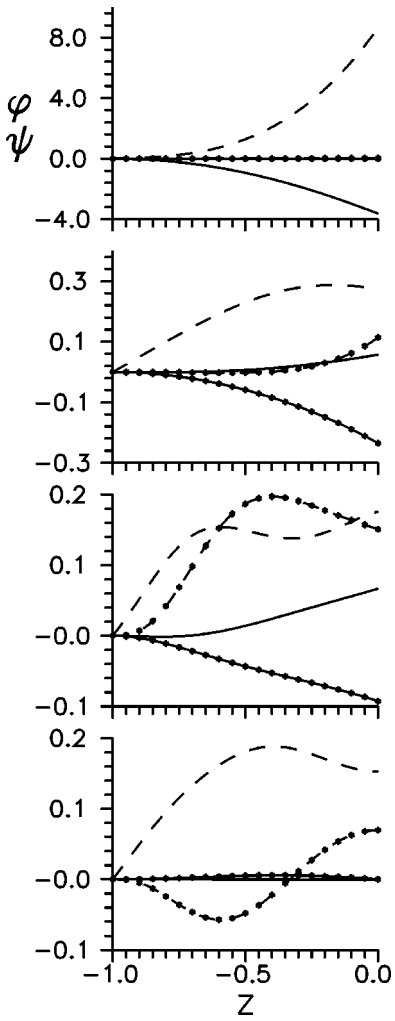

FIG. 5. Graphs of the functions ϕ and ψ with respect to z along the thickness of the fluid layer. The solid curves are the real part of ϕ and the dashed ones are the real part of ψ. The starred curves (solid and dashed) correspond to the imaginary parts. The first figure is for $\Omega=1.75$, $\mathrm{Re}_c=54.48$, $\varepsilon=143.7$, $c=9.788$, $G=16.56$, $a\to 0$; the second is for $\Omega=2$, $\mathrm{Re}_c=72.36$, $\varepsilon=103.55$, $c=27.22$, $G=19.25$, $a=0.3446$; and the third is for $\Omega=20$, $\mathrm{Re}_c=10\,427.68$, $\varepsilon=223.6$, $c=-22.81$, $G=277.42$, $a=0.2863$. All three figures are for $\gamma=20°$, $\hat{\gamma}=30°$, $\Sigma=500$. The fourth figure is for $\gamma=0°$, $\hat{\gamma}=30°$, $\Sigma=500\,000$ and has $\Omega=7.5$, $\mathrm{Re}_c=3095.08$, $\varepsilon=15.97$, $c=89.01$, $a=0.965$. This one presents profiles corresponding to the Ekman boundary layer which destabilizes at a small angle ε.

If in addition $\gamma=0$, the angle of propagation minimizing Re_c is

$$\tan 2\varepsilon=\frac{30}{7}\chi^2 \tag{22}$$

as found by Charwat *et al.* [14]. However, when $\gamma\neq 0$, the minimum is given by

$$\tan 2\varepsilon=q-q_1\sqrt{1+\tan^2 2\varepsilon} \tag{23}$$

whose solution is

$$\tan 2\varepsilon = \frac{q - q_1\sqrt{1+q^2-q_1^2}}{1-q_1^2} \tag{24}$$

with $q_1 = 9\chi^2 \tan\gamma \tan\hat{\gamma}/40$ and $q = 30\chi^2/7 - q_1$.

Expression (24) reduces to Eq. (22) in the limit $\gamma \to 0$. The condition that the radicand in expression (24) remains positive

$$\tan\hat{\gamma} < \frac{1 + (\frac{30}{7}\chi^2)^2}{\frac{9}{20}\chi^2 \tan\gamma(\frac{30}{7}\chi^2)} \tag{25}$$

yields an upper bound for the angle $\hat{\gamma}$.

Though usually positive angles ε are found at finite rotation rates, it is possible to find the onset of disturbances with $\varepsilon < 0$ as shown in Fig. 4(b). Accordingly to expression (24) positive angles ε are obtained for

$$\tan\hat{\gamma} < \frac{200}{21\tan\gamma}. \tag{26}$$

For example, in the case $\hat{\gamma} = 87°$, $\gamma < 26.52°$ is required for positive ε, while ε becomes negative for larger inclinations. The reason for the appearance of negative angles probably can be explained as done by Dávalos-Orozco and Ruiz-Chavarría [19] for the case of a rotating vertical plane under slow rotation.

The parameter values $\hat{\gamma} = 87°$ and $\Sigma = 2500$ in Fig. 4 have been chosen since they are close to those of the experiments by Leneweit *et al.* [18] at large distances from the rotation axis. The critical Reynolds number is shown in Fig. 4(a). Note that the differences in stability between the inclined and horizontal plane are more marked than in the other figures.

IV. EKMAN BOUNDARY LAYER INSTABILITY

Besides the instabilities which depend on distortion of the free surface of the film there are other instabilities which occur also in the absence of free surface. The analog of the Tollmien-Schlichting-type instability in channel flow can usually be neglected since it occurs at rather high Reynolds numbers. But shear flows in rotating systems typically exhibit Ekman layer instabilities which could be relevant since their critical Reynolds numbers are usually lower. An attempt has thus been made to find Ekman layer instabilities in cases of high surface tension when a distortion of the surface is strongly inhibited for finite wave numbers a. Using $\Sigma = 5 \times 10^5$, $\gamma = 0$, $\hat{\gamma} = 30$ we found the following results:

$\Omega = 2.5$, $G_c = 426.5$, $\varepsilon = -16.9°$, $a = 0.945$ $c = 66.4$,

$\Omega = 5$, $G_c = 240.4$, $\varepsilon = 4.1°$, $a = 0.966$, $c = 74.2$,

$\Omega = 7.5$, $G_c = 206.4$, $\varepsilon = 16.0°$, $a = 0.965$, $c = 89.0$,

where G is defined below Eq. (16). These results agree quite well with those of Gusev and Bark [22] (see also Ref. [23]) who have determined the onset of Ekman instability of type II or A in a channel flow in a system rotating about an axis normal to the wall. We have used G here instead of the Reynolds number Re defined below Eq. (9) since G corresponds to the Reynolds number used by Gusev and Bark. The Reynolds number for the onset of the surface instability is still lower and the critical values $G_c = 77.7$, 99.2, and 120.7 at $\Omega = 2.5$, 5, and 7.5, respectively, are attained at much lower values of a for $\Sigma = 5 \times 10^5$. But since the two instabilities do not interfere much with each other, they may eventually be observed simultaneously.

V. NONLINEAR WAVE EQUATION

In this section a nonlinear wave equation for the surface deformation is derived. To reach that goal, it is necessary to rescale Eqs. (7) to (15) in a way convenient for the small wave number and the small χ approximation. Let δ be a small parameter [10] which is proportional to the ratio of the thin film thickness d and a representative disturbance wavelength l_0, that is, $\delta \sim d/l_0$. By means of δ the independent variables are scaled as $x = \delta x'$, $y = \delta y'$, $z = z'$, and $t = \delta t'$. Note that in this calculation the solid plane will be supposed located at $z = 0$ and the free surface at $z = h$, where $h = 1 + H$.

The dependent variables are expanded [14] with respect to the two parameters δ and χ

$$u = u_{00} + \delta u_{10} + \chi^2 u_{01} + \delta\chi^2 u_{11} + \cdots, \tag{28}$$

with analogous expansions for v, $\delta^{-1}w$, and p.

In this way, following the procedure [3,2,8,9,10] for the derivation of the Benney equation, an equation describing three-dimensional waves is obtained,

$$\begin{aligned} & h_t + \mathrm{Re}(h^2 h_x - \tfrac{4}{3}\chi^2 h^4 h_y) + \delta\{\tfrac{2}{15}\mathrm{Re}^2(h^6 h_x)_x \\ & \quad - \tfrac{1}{3}\vec{\nabla}\cdot[\mathrm{Re}\cot\hat{\gamma} h^3 \vec{\nabla} h - Sh^3\vec{\nabla}(\nabla^2 h)]\} + \delta\chi^2 \\ & \quad \times[-(\tfrac{4}{7}\mathrm{Re}^2 h^8 h_x - \tfrac{3}{20}\mathrm{Re}\tan\gamma h^5 h_x)_y + \mathrm{Re}\vec{\nabla}\cdot(\tfrac{5}{6}h^5 h_y \vec{\nabla} h \\ & \quad + \tfrac{8}{45}h^6\vec{\nabla}h_y) - \tfrac{4}{3}Sh^4(h_y\nabla^2 h_x - h_x\nabla^2 h_y)] \\ & = 0, \end{aligned} \tag{29}$$

where $S = \Sigma\delta^2$. Besides, $\vec{\nabla} = (\partial/\partial_x, \partial/\partial_y)$, $\nabla^2 = \partial^2/\partial x^2 + \partial^2/\partial y^2$ and subindexes t, x, and y indicate partial derivatives. This equation reduces to that obtained by Roskes [24] (note the different nondimensional parameters) and by Joo and Davis [9] when $\chi^2 = 0$.

Now, a rotation by the angle ε of the coordinate system is done

$$\begin{aligned} x' &= x\cos\varepsilon - y\sin\varepsilon, \\ y' &= x\sin\varepsilon + y\cos\varepsilon, \end{aligned} \tag{30}$$

such that the disturbances depend on x' but no longer on y'.

Accordingly, the equation for the surface deformation transforms into

$$h_t+\frac{\partial}{\partial x}\{R(\tfrac{1}{3}h^3\cos\varepsilon+\tfrac{4}{15}\chi^2h^5\sin\varepsilon)+\delta[\tfrac{2}{15}\mathrm{Re}^2\cos^2\varepsilon h^6h_x - \tfrac{1}{3}(R\cot\hat{\gamma}h^3h_x-Sh^3h_{xxx})] + \chi^2\delta[\sin\varepsilon\cos\varepsilon(\tfrac{4}{7}R^2h^8h_x-\tfrac{3}{20}\mathrm{Re}\tan\gamma h^5h_x) - \mathrm{Re}\sin\varepsilon(\tfrac{5}{6}h^5h_x^2+\tfrac{8}{45}h^6h_{xx})]\}=0, \quad (31)$$

where the primes have been omitted in order to simplify the notation. Obviously this equation has the form of a mass conservation equation:

$$h_t+\mathbf{Q}_x=0, \quad (32)$$

where $\mathbf{Q}$ represents the terms inside the curly brackets.

The linearization of Eq. (31) leads to the results of Eqs. (18) and (19) presented in Sec. III when use is made of normal modes which are assumed such that δh_x and $\delta^{-1}h_t$ are replaced by iah and $(-iac+\Gamma)h$, respectively. Note that the last term of Eq. (31) is the dispersion term which corresponds to the last one of the phase velocity in Eq. (18).

Assuming spatial periodicity with a wave number a the solution of Eq. (31) can be analyzed in the form

$$h=1+\sum_m [A_m(t)\exp\{i\ \ m\ \ a\ \ x\}+\text{c.c.}], \quad (33)$$

where c.c. means complex conjugate and the complex amplitudes $A_m(t)$ can be written in the form $A_m(t)=|A_m(t)|\exp\{i\theta_m\}$. Restricting the attention to just two of these amplitudes [25] we obtain

$$\frac{d|A_1|}{dt}=-C_{1r}|A_1|-C_{2r}|A_1|^3-(C_{3r}\cos\Delta_1 - C_{3i}\sin\Delta_1)|A_1||A_2|, \quad (34)$$

$$\frac{d|A_2|}{dt}=-C_{5r}|A_2|-(C_{4r}\cos\Delta_1+C_{4i}\sin\Delta_1)|A_1|^2, \quad (35)$$

$$\frac{d\Delta_1}{dt}=-6B_9-(C_{4i}\cos\Delta_1-C_{4r}\sin\Delta_1)\frac{|A_1|^2}{|A_2|}, \quad (36)$$

where $\Delta_1=\theta_2-2\theta_1$ and the subscripts r and i refer to the real and imaginary parts of the coefficients, respectively. The coefficients C_m $(m=1,...,5)$ and B_9 are given in the Appendix.

The purpose of these coupled nonlinear amplitude equations is twofold. First they allow us to determine the saturation of the amplitude A_1 of the wave in dependence of the Reynolds number Re. For a given value of the wave number a the growth rate is negative for low values of Re. With increasing Re the growth rate vanishes when the relation

$$a_c=\sqrt{3/S}\sqrt{\mathrm{Re}^2(\tfrac{2}{15}\cos^2\varepsilon+\tfrac{4}{7}\chi^2\sin\varepsilon\cos\varepsilon)-\mathrm{Re}(\tfrac{1}{3}\cot\hat{\gamma}+\tfrac{3}{20}\chi^2\tan\gamma\sin\varepsilon\cos\varepsilon)} \quad (37)$$

is satisfied and it becomes positive for higher values of Re. This relation describes the curve of criticality in a plot of a_c against Re. Below the curve of criticality the wave grows until saturation is attained. In this case, steady equilibria with

$$|A_1|^2=\frac{C_{1r}C_{5r}}{(C_{3r}\cos\Delta_1-C_{3i}\sin\Delta_1)(C_{7r}\cos\Delta_1+C_{7i}\sin\Delta_1)-C_{2r}C_{5r}}, \quad (38)$$

$$|A_2|=-(C_{7r}\cos\Delta_1+C_{7i}\sin\Delta_1)A_1^2/C_{5r}, \quad (39)$$

$$\tan\Delta_1=\frac{-6B_9C_{7r}+C_{5r}C_{7i}}{C_{5r}C_{7r}+6B_9C_{7i}} \quad (40)$$

are possible according to the vanishing of the right-hand sides of Eqs. (34), (35), and (36). Note that these equations are only meaningful as long as $|A_2|\ll|A_1|^2$ is satisfied since otherwise the amplitudes of higher harmonics can no longer be neglected. This condition has actually been used in Eq. (35) in order to neglect terms of higher order.

The expression left on the right-hand side of Eq. (38) without C_{5r} was analyzed numerically. It was found that it is positive in a range of Reynolds numbers not too far from criticality. Therefore, C_{5r} should be positive and the curve of subcriticality is determined by the locus of the points in parameter space where C_{5r} changes sign. In a plot of a_s against Re, where a_s is the wave number of subcriticality, the wave does not saturate in the above approximation for $a<a_s$ for a fixed Re or for Reynolds numbers larger than those of the curve of subcriticality when the wave number is fixed. Crossing the curve of subcriticality C_{5r} becomes negative. In this way, the approximate curve of subcriticality for the first two Fourier modes is defined by $C_{5r}=0$ or by

$$a_s=\tfrac{1}{2}a_c, \quad (41)$$

which reduces to that of Gjevik [25] when $\Omega=0$. Note that C_{1r} is the negative of the growth rate and that C_{5r} is the

negative of the constant β_{2r} used by Gjevic. It is important to point out that condition Eq. (41) does not restrict, in the small region between a_c and a_s, the evolution of the waves described by Eq. (31). In fact, in the case of $\Omega=0$, it has been shown by Dávalos-Orozco *et al.* [10] through the use of finite differences and by Joo *et al.* [8,26] with Fourier spectral methods that saturation may be found still far away from the curve of subcriticality. However, Eq. (41) gives an approximation to the limitations of the theory. Besides, it guarantees that saturation occurs in the area below a_c and above a_s.

The second purpose of Eqs. (34)–(36) is to show that the linearized version of Eq. (34) contains the growth rate $-C_{1r}$ and that the imaginary part of C_1 equals *ac* as given in Eq. (18).

When the small wave amplitude assumption is introduced,

$$H_t + c_l H_x + c_n H H_x + \delta\beta_1 H_{xx} - \delta\beta_2 H_{xxx} + \delta\beta_3 H_{xxxx} = 0 \tag{42}$$

is obtained from Eq. (31), where

$$c_l = \mathrm{Re}(\cos\varepsilon + \tfrac{4}{3}\chi^2 \sin\varepsilon), \quad c_n = 2\,\mathrm{Re}(\cos\varepsilon + \tfrac{8}{3}\chi^2 \sin\varepsilon), \tag{43}$$

$$\beta_1 = \tfrac{2}{15}\mathrm{Re}^2 \cos^2\varepsilon - \tfrac{1}{3}\mathrm{Re}\cot\hat{\gamma} + \chi^2 \sin\varepsilon\cos\varepsilon(\tfrac{4}{7}\mathrm{Re}^2 - \tfrac{3}{20}\mathrm{Re}\tan\gamma), \tag{44}$$

$$\beta_2 = \tfrac{8}{15}\chi^2 \mathrm{Re}\sin\varepsilon, \quad \beta_3 = \tfrac{1}{3}S \tag{45}$$

have been used. This equation reduces to the Kuramoto-Sivashinsky equation [4,5] for $\beta_2=0$. The equation with a positive dispersion term has been shown by Kudriashov and Zargaryan [27], Fan [28] and others to admit exact solitary wave solutions. Fan [28] also has shown that it admits solitary wave solutions when the sign of dispersion is negative, as in the present case. A complete numerical investigation of the properties of Eq. (42) for positive or negative dispersion term has been done by Chang *et al.* [29]. In that paper, the branches for the appearance of solitary waves are investigated and the shapes of the waves corresponding to each of the different branches are presented.

Assuming, that the spiral waves shown in the photographs of Leneweit *et al.* [18] are solitary waves we can calculate the phase velocity based on Fig. 3 of Chang *et al.* [29]. To use the results of Chang *et al.* [29], it is necessary to first transform Eq. (42) to a one parameter equation. By means of $H=(\zeta-c_l)/c_n$ the amplitude is transformed, where $c_n\neq 0$, in order to obtain

$$\zeta_t + \zeta\zeta_x + \delta\beta_1\zeta_{xx} - \delta\beta_2\zeta_{xxx} + \delta\beta_3\zeta_{xxxx} = 0. \tag{46}$$

Further, this equation is transformed into a system where the wave is stationary, $\partial/\partial t \to \partial/\partial t - b\,\partial/\partial x$, where b is the velocity of that system. Then, the following stretched variables: $\zeta=\delta\beta_1\sqrt{\beta_1/\beta_3}\,\xi$, $x=\sqrt{\beta_3/\beta_1}\,x'$, $t=(\beta_3/\delta\beta_1^2)t'$, $\overline{\sigma}=\beta_2/\sqrt{\beta_1\beta_3}$, and $\overline{c}=b/\sqrt{\delta^2\beta_1^3/\beta_3}$ are introduced, yielding

$$-\overline{c} + \xi\xi_{x'} + \xi_{x'x'} - \overline{\sigma}\xi_{x'x'x'} + \xi_{x'x'x'x'} = 0 \tag{47}$$

as the final equation. The parameters $\overline{c}$ and $\overline{\sigma}$ correspond to the velocity λ and parameter $-\delta$ in Fig. 3 of Chang *et al.* [29]. In the case of the experiments [18] the parameter $\overline{\sigma}$ is very small. However, according to its definition and Eq. (44), $\overline{\sigma}$ increases when the Reynolds number approaches criticality in the absence of surface tension [see Eq. (21)]. Since solitary waves do not occur for $\overline{\sigma}$ larger than a value around 0.4 (in the case of branch *b* in Fig. 3 of Chang *et al.* [29]), we conclude that solitary waves are possible only for relatively large Reynolds numbers.

Note that the derivation of Eq. (47) has been general, taking into account all allowed angles of inclination. In order to predict the behavior of the phase velocity for future experiments we assume that $\gamma=0$ and select the data of Leneweit *et al.* [18] corresponding to a flow flux $Q=0.5$. The magnitude of $\overline{c}$ is taken from Fig. 3 of Chang *et al.* [29] in which the branch *b* of the figure has been selected because the associated surface profiles seem to be most similar to those shown in the photographs of Leneweit *et al.* [18].

The phase velocity c_t of the spiral waves, shown for $Q=0.5$ in Table I, decreases with distance from the axis of rotation. Note that the phase velocity in the table is given in the same nondimensional way as in Ref. [18]. Calculations made for different values of Q also show the decrease with distance from the axis. This agrees with comments made by Azuma and Nunobe [17] who say (see p. 2145), ''Now, when the variation of ϕ (here ε) and u_d (the phase velocity) was investigated for each rotation frequency and in a range of 80 to 90 mm, it was observed that ϕ has some decrease with the radius and also u_d has some decrease in the same direction.''

VI. CONCLUSIONS

The main results of this paper are that the usual surface wave instability of a fluid film flowing down an inclined plate is only slightly modified in a rotating system as long as the rotation rate is small. Only the direction of propagation of the wave is turned, usually in a direction opposite to that of rotation. When the rotation rate exceeds a critical value, however, a new instability occurs, characterized by a finite value of the critical wave number. Given a direction of the effective gravity force, the flow for large rotation rates is more unstable when the plate is inclined in contrast to the case of low rotation limit where the opposite situation prevails. The Ekman layer instability has also been considered. But except in unusual situations it will not precede the surface wave instabilities.

A three-dimensional nonlinear wave equation, generalizing Roskes' [24] equation has been derived. The two-dimensional version generalizes the equation obtained by Benney [3]. From the resultant equation, two equations were derived corresponding to the amplitudes of the first two Fourier modes of the surface deformation. From this set of equations a condition for wave saturation can be obtained.

For small amplitudes the two-dimensional nonlinear wave equation reduces into an equation which differs from the Kuramoto-Sivashinski equation only by the dispersion term. Transforming Eq. (40) and using stretched variables we have obtained the velocity of the solitary wave in terms of the

TABLE I. Prediction of the phase velocity for future experiments. The flow flux selected is $Q=0.5$. The data presented were obtained using the formula $d/r=0.701\,13\,(Q\nu/|\vec{\Omega}|^2 r^5)^{0.3287}$ obtained from Fig. 5 of the paper of Leneweit *et al.* [18]. To determine the nondimensional parameters, use was made of $\rho=998.2$ kg/m^3, $\nu=1.007\times10^{-6}$ m^2/sec, and $\sigma=7.36\times10^{-2}$ N/m of water at 20 °C. In the experiments [18], radial distances are measured in units of $l=(9Q^2/4\pi^2\nu\omega)^{1/4}$. The columns of the table are organized as follows. First column: the flow flux Q; second column: radial distance r from the axis in centimeters and in l units; third column: the angle $\hat{\gamma}$ ($\gamma=0$); fourth column: experimental Reynolds number Re; fifth column: the linear critical Reynolds number for $a\to0$; sixth column: the linear critical Reynolds number when $a=0.065$ (as observed in the experiments [14,18]); seventh column: the capillary number Σ (note $S=\Sigma\delta^2$ and $\delta=0.1$, always); eighth column: the rotation parameter Ω; ninth column: the linear critical ε; tenth column: the dispersion parameter $\overline{\sigma}$ of Eq. (47); eleventh column: the linear phase velocity c_{ph} calculated from Eq. (18); twelfth column: the solitary wave velocity c_s obtained using Eq. (47); and the thirteenth column: the total phase velocity obtained by adding the eleventh and twelfth columns. The velocities are given here in the nondimensional form of Ref. [18].

Q (m/sec)	r (units of 10^{-2} m)	H (units of 10^{-5} m)	$\hat{\gamma}$	Re	Re_c ($a\to0$)	Re_c ($\alpha=0.065$)	Σ	Ω	ε	$\overline{\sigma}$ (units of 10^{-3})	c_{ph}	c_s	c_t
0.5	4.383(81)	3.129	86.7582	5.409	0.1393	0.5607	2274.8	0.061 07	7.334	2.95	2.004 10	0.1275	2.1310
0.5	4.931(91)	2.900	87.1148	4.808	0.1244	0.5353	2108.8	0.052 48	6.338	3.21	2.003 23	0.1048	2.1080
0.5	6.026(111)	2.549	87.6387	3.934	0.1023	0.4949	1853.3	0.0405	4.923	2.06	2.001 89	0.0739	2.0758
0.5	7.669(141)	2.182	88.1440	3.091	0.0806	0.4509	1586.9	0.0297	3.627	1.21	2.001 01	0.0492	2.0502

parameters deduced from the experiment and shown in Table I. This solitary wave velocity was added to the linear phase velocity to give the total velocity of the wave. The conclusions are that, for each flow flux, the wave velocity decreases with distance from the rotation axis. This result agrees with the experimental results by Azuma and Nunobe [17]. But convincing agreement with the measurements of the phase velocity by Leneweit *et al.* [18] could not be attained. A reason for this disagreement could be the indirect way in which the phase velocity was measured in the experiment. They found at some radial interval that the phase velocity first increases and later decreases. Farther away they observe, for different flow fluxes, that the phase velocity increases monotonically at some interval after which it attains a nearly constant magnitude. It should be noted that the experimental results depend on the flow flux and on the perturbations at the inlet. The frequency of those perturbations is unknown but it seems that changes are found varying the height of the inlet. Therefore, the experimental results are not conclusive. With Table I our purpose is to set, theoretically, the possible behavior of the phase velocity of spiral waves with respect to the radial distance using data taken directly from an experiment. Moreover, Table I can be used to check with future experimental data.

ACKNOWLEDGMENTS

L.A.D.-O. would like to thank the Institute of Physics, University Bayreuth, for their hospitality. Thanks are also due to DGAPA-UNAM for support to project No. IN119200.

APPENDIX: COEFFICIENTS OF EQS. (34)–(36)

The coefficients will be written in terms of the B_i parameter groups. They are

$$C_1=3iaB_1+5iaB_2-a^2B_3+a^2B_4+a^4B_5-a^2B_6+a^2B_7+ia^3B_9, \tag{A1}$$

$$C_2=3iaB_1+30iaB_2-15a^2B_3+3a^2B_4+3a^4B_5-28a^2B_6+10a^2B_7-5ia^3B_8+45ia^3B_9, \tag{A2}$$

$$C_3=6iaB_1+20iaB_2-6a^2B_3+3a^2B_4+21a^4B_5-8a^2B_6+5a^2B_7-4ia^3B_8+30ia^3B_9, \tag{A3}$$

$$C_4=6iaB_1+20iaB_2-12a^2B_3+6a^2B_4+6a^4B_5-16a^2B_6+10a^2B_7+2ia^3B_8+12ia^3B_9, \tag{A4}$$

$$C_5=6iaB_1+10iaB_2-4a^2B_3+4a^2B_4+16a^4B_5-4a^2B_6+4a^2B_7+8ia^3B_9, \tag{A5}$$

$$B_1=\tfrac{1}{3}\mathrm{Re}\cos\varepsilon,\quad B_2=\tfrac{4}{15}\mathrm{Re}\chi^2\sin\varepsilon,$$
$$B_3=\tfrac{2}{15}\delta\mathrm{Re}^2\cos^2\varepsilon,\quad B_4=\tfrac{1}{3}\delta\mathrm{Re}\cot\hat{\gamma},\quad B_5=\tfrac{1}{3}\delta S, \tag{A6}$$

$$B_6=\frac{4}{7}\delta\chi^2\mathrm{Re}^2\sin\varepsilon\cos\varepsilon,\quad B_7=\tfrac{3}{20}\delta\chi^2\mathrm{Re}\tan\gamma\sin\varepsilon\cos\varepsilon,$$
$$B_8=\tfrac{5}{6}\delta\chi^2\mathrm{Re}\sin\varepsilon=\tfrac{75}{16}B_9. \tag{A7}$$

[1] T. B. Benjamin, J. Fluid Mech. **2**, 554 (1957).
[2] C. S. Yih, Phys. Fluids **6**, 321 (1963).
[3] D. J. Benney, J. Math. Phys. **45**, 150 (1966).
[4] Y. Kuramoto and T. Tsuzuki, Prog. Theor. Phys. **55**, 356 (1976).
[5] G. Sivashinsky, Acta Astron. **4**, 1177 (1977).
[6] A. Pumir, P. Manneville, and Y. Pomeau, J. Fluid Mech. **135**, 27 (1983).
[7] C. Nakaya, Phys. Fluids A **1**, 1143 (1989).

[8] S. W. Joo, S. H. Davis, and S. G. Bankoff, J. Fluid Mech. **230**, 117 (1991).
[9] S. W. Joo and S. H. Davis, J. Fluid Mech. **242**, 529 (1992).
[10] L. A. Dávalos-Orozco, S. H. Davis, and S. G. Bankoff, Phys. Rev. E **55**, 374 (1997).
[11] J. Liu and J. P. Gollub, Phys. Rev. Lett. **70**, 2289 (1993).
[12] J. Liu and J. P. Gollub, Phys. Fluids **6**, 1702 (1994).
[13] J. Liu, J. B. Schneider, and J. P. Gollub, Phys. Fluids **7**, 55 (1995).
[14] A. F. Charwat, R. E. Kelly, and C. Gazley, J. Fluid Mech. **53**, 227 (1972).
[15] J. W. Rauscher, R. E. Kelly, and J. D. Cole, J. Appl. Mech. **40**, 43 (1973).
[16] D. J. Needham and J. H. Merkin, J. Fluid Mech. **184**, 357 (1987).
[17] T. Azuma and M. Nunobe, Trans. Jpn. Soc. Mech. Eng., Ser. B **55**, 2139 (1989) (in Japanese).
[18] G. Leneweit, K. G. Roesner, and R. Koehler, Exp. Fluids **26**, 75 (1999).
[19] L. A. Dávalos-Orozco and G. Ruiz-Chavarría, Phys. Fluids A **4**, 1651 (1992).
[20] N. P. Hoffmann and F. H. Busse, Phys. Fluids **11**, 1676 (1999).
[21] W. H. Press, B. P. Flannery, S. A. Teukolsky, and W. T. Vetterling, *Numerical Recipes*, 2nd ed (Cambridge University Press, Cambridge, 1992).
[22] A. Gusev and F. H. Bark, Phys. Fluids **23**, 2171 (1980).
[23] N. P. Hoffmann and F. H. Busse, Phys. Fluids **13**, 2735 (2001).
[24] G. J. Roskes, Phys. Fluids **13**, 1440 (1970).
[25] B. Gjevik, Phys. Fluids **13**, 1918 (1970).
[26] S. W. Joo (private communication).
[27] N. A. Kudraishov and E. D. Zargaryan, J. Phys. A **29**, 8067 (1996).
[28] E. Fan, Phys. Lett. A **277**, 212 (2000).
[29] H.-C. Chang, E. A. Demekhin, and D. I. Kopelevich, Physica D **63**, 299 (1993).